Available online at www.sciencedirect.com
SCIENCE DIRECT
Journal of Molecular Graphics and Modelling 24 (2006) 262–270
Journal of Molecular Graphics and Modelling
www.elsevier.com/locate/JMGM

A reactivity index study to rationalize the effect of dopants on Brönsted and Lewis acidity occurring in MeAlPOs

Abhijit Chatterjee *

Department of Material Science, Accelrys, Nishishinbashi TS Bldg. 11F, 3-3-1 Nishishinbashi, Minato-ku, Tokyo 105-0003, Japan

Received 2 June 2005; received in revised form 9 September 2005; accepted 9 September 2005
Available online 21 October 2005

Abstract

The influence of both bivalent and trivalent metal substituents from a range of metal cation (Co, Mn, Mg, Fe and Cr) on the acidic property (both Brönsted and Lewis) of metal substituted aluminum phosphate MeAlPOs is monitored. The influence of the environment of the acid site is studied both by localized cluster and periodic calculations to propose that the acidity of AlPOs can be predictable with accuracy so that AlPO material with desired acidity can be designed. A semi-quantitative reactivity scale within the domain of hard soft acid–base (HSAB) principle is proposed in terms of the metal substitutions using density functional theory (DFT). It is observed that for the bivalent metal cations Lewis acidity linearly increases with ionic size, where as the Brönsted acidity is solely dependent on the nearest oxygen environment. Intramolecular and intermolecular interactions show that once active site of the interacting species is identified, the influence of the environment can be prescribed. Mg(II)-doped AlPO-34 shows highest Brönsted acidity and whereas Cr(III)-doped species shows lowest acidity. Fe(II)/Fe(III)-doped AlPO-34 shows highest Lewis acidity, whereas Mn(III), Mg (II) shows lowest acidity.

Keywords: Dopants; Brönsted acidity; Lewis acidity; MeAlPOs; Reactivity index; DFT

1. Introduction

Aluiminophospahates (AlPOs) are crystalline microporous molecular sieves. They are made up from alternating AlO_4 and PO_4 tetrahedra, connected through corner sharing of oxygen atoms. These tetrahedral moieties then form a three-dimensional network containing channels and pores. AlPOs are structurally analogous to the type of aluminosilicate zeolites, where the Si^{4+} can be substituted by P^{4+} to have an alternate arrangement of Al and P. AlPOs, though a structural analog of zeolite the show a better flexibility than zeolites towards chemical substitution [1], to which they have been shown to support acid and/or redox activity in the microporous materials [2–4]. AlPOs show Brönsted acidity when acid protons neutralize the charge resulted from a substitution by a lower valent metal ion in the framework. Transition metal substituted AlPOs (MeAlPOs) have shown a marked tendency to Lewis acidity as well associated with the metal dopants [5]. The metal-doped AlPOs have widespread application in the field of heterogeneous catalysis especially in oxidation of hydrocarbons [6]. The acid strength and catalytic activity, however depends on the type of metal dopants employed. There are many experimental studies, which have investigated the correlation between acidity and the local structure of the active site, and nature of metal dopant in the AlPOs [7–9]. MeAlPOs doped with transition metals due to their flexible oxidation state can play a prominent role in selective oxidation of hydrocarbons [10]. In a recent study of Saadoune et al. [11,12] have done a study on structural and electronic properties of dopant ions in AlPOs. They have shown that the acid strength of AlPOs is dependent on a complex combination of structural and electronic features of the dopant ions and does not have any considerable contribution from the local environment of the dopant cations both for bivalent and trivalent state in the framework. This is as well a little contradictory from their earlier views [13], where they proposed that larger the difference in ionic radius between the host ion and the dopant, the more site ordered phases become energetically stable. They have used Hartree–Fock label theory, which is inferior to the quality we were using in terms of predicting the geometry; which is important to interpret the effect of neighboring atoms in the real architecture,

* Tel.: +81 3 3578 3861; fax: +81 3 3578 3873.
E-mail address: achatterjee@accelrys.com.

1093-3263/$ – see front matter © 2005 Elsevier Inc. All rights reserved.
doi:10.1016/j.jmgm.2005.09.003

as well they were unable to propose an activity order for these dopants. We therefore wish to probe into these facts of the activity of the cations and the influence of local architecture of the framework on their said activity and look into the fact that whether the acidity in AlPO is really unaccounted for, which the other group has demanded. This is very important in terms of catalytic reactions, where the experimentalists wanted to use materials with varying acid strength for typical reactions. This will open an area of material designing.

The hard soft acid–base (HSAB) principles classify the interaction between acids and bases in terms of global softness. Pearson proposed the global HSAB principle [14]. The global hardness was defined as the second derivative of energy with respect to the number of electrons at constant temperature and external potential, which includes the nuclear field. The global softness is the inverse of this. Pearson also suggested a principle of maximum hardness (PMH) [15], which states that, for a constant external potential, the system with the maximum global hardness is most stable. In recent days, DFT has gained widespread use in quantum chemistry. Some DFT-based local properties, e.g. Fukui functions and local softness [16], have already been used for reliable predictions in various types of electrophilic and nucleophilic reactions [17–20]. Moreover, Gazquez and Mendez [21], proposed that when two molecules A and B of equal softness interact, thereby implicitly assuming one of the species as nucleophile and the other as an electrophile, then a novel bond would likely form between an atom A and an atom B whose Fukui function values are close to each other. In our study [20] we proposed a reactivity index scale for heteroatomic interaction with zeolite framework. The scale holds well for unisite interaction or in other way with one active site preset in the molecule, the scale does not hold good for systems with two or more active sites. So far there are many theoretical studies with the influence of zeolite structure and composition on acid strength [22,23]. There is a scant literature using reactivity descriptors [24]. A recent paper of Deka et al. [25] has dealt the issue with only monovalent cations.

With this background we performed first ab intio periodic calculation to monitor the role of the framework on the activity of dopants in MeAlPOs. We have performed a systematic study with metal dopants at their different oxidation state: Co^{2+}, Co^{3+}; Mn^{2+}, Mn^{3+}; Mg^{2+}; Fe^{2+}, Fe^{3+} and Cr^{2+}, Cr^{3+}. The trend observed through periodic calculation is validated by localized cluster calculation using localized reactivity index parameters to look into the localized interaction of these dopants with varying charge. Finally a semi-quantitative scale is proposed for the first time in terms of the activity of the dopants both in terms of Brönsted and Lewis acidity.

2. Theory

In density functional theory, hardness (η) is defined as [26]:

$$\eta = \frac{1}{2}\left(\frac{\delta^2 E}{\delta N^2}\right)v(r) = \frac{1}{2}\left(\frac{\delta\mu}{\delta N}\right)_v \tag{1}$$

where E is the total energy, N is the number of electrons of the chemical species and the chemical potential.

The global softness, S, is defined as the inverse of the global hardness, η.

$$S = \frac{1}{2\eta} = \left(\frac{\delta N}{\delta\mu}\right)_v \tag{2}$$

Using the finite difference approximation, S can be approximated as

$$S = \frac{1}{\mathrm{IE} - \mathrm{EA}} \tag{3}$$

where IE and EA are the first ionization energy and electron affinity of the molecule, respectively.

The Fukui function $f(r)$ is defined by [16]

$$f(r) = \left[\frac{\delta\mu}{\delta v(r)}\right]_N = \left[\frac{\delta\rho(r)}{\delta N}\right]_v \tag{4}$$

The function 'f' is thus a local quantity, which has different values at different points in the species, N is the total number of electrons, μ the chemical potential and v the potential acting on an electron due to all nuclei present. Since $\rho(r)$ as a function of N has slope discontinuities, Eq. (1) provides the following three reaction indices [16]:

$$f^-(r) = \left[\frac{\delta\rho(r)}{\delta N}\right]_v^- \quad \text{(governing electrophilic attack)},$$

$$f^+(r) = \left[\frac{\delta\rho(r)}{\delta N}\right]_v^+ \quad \text{(governing nucleophilic attack)},$$

$$f^0(r) = \tfrac{1}{2}[f^+(r) + f^-(r)] \quad \text{(for radial attack)}$$

In a finite difference approximation, the condensed Fukui function [26] of an atom, say x, in a molecule with N electrons are defined as:

$$\begin{aligned} f_x^+ &= [q_x(N+1) - q_x(N)] \quad \text{(for nucleophilic attack)},\\ f_x^- &= [q_x(N) - q_x(N-1)] \quad \text{(for electrophilic attack)},\\ f_x^0 &= \tfrac{1}{2}[q_x(N+1) - q_x(N-1)] \quad \text{(for radical attack)} \end{aligned} \tag{5}$$

where q_x is the electronic population of atom x in a molecule.

The local softness $s(r)$ can be defined as

$$s(r) = \left(\frac{\delta\rho(r)}{\delta\mu}\right)_v \tag{6}$$

Eq. (3) can also be written as

$$s(r) = \left[\frac{\delta\rho(r)}{\delta N}\right]v\left[\frac{\delta N}{\delta\mu}\right]_v = f(r)S \tag{7}$$

Thus, local softness contains the same information as the Fukui function $f(r)$ plus additional information about the total molecular softness, which is related to the global reactivity

with respect to a reaction partner, as stated in HSAB principle. Atomic softness values can easily be calculated by using Eq. (4), namely:

$$s_x^+ = [q_x(N+1) - q_x(N)]S, \qquad s_x^- = [q_x(N) - q_x(N-1)]S,$$
$$s_x^0 = \frac{S[q_x(N+1) - q_x(N-1)]}{2} \tag{8}$$

3. Computational methodology and model

Ab initio total energy pseudopotential calculations were performed using CASTEP (Cambridge Serial Total Energy Package), and associated programs of Accelrys, which has been described elsewhere [27,28] for all the calculations with imposed periodic boundary conditions. In this code, the wave functions of valence electrons are expanded in a basis set of plane waves with kinetic energy smaller than a specified cut of energy, E_{cut}. The presence of tightly bound core electrons is represented by nonlocal ultra soft pseudopotentials [29]. CASTEP is a pseudopotential total energy code that employs Perdew and Zunger [30] parameterization of the exchange-correlation energy, super cells and special point integration over the Brillouin zone and a plane wave basis set for the expansion of wave functions. The methodology has been used in mineralogy to examine the hydration of corderite [31]. Becke–Perdew parametrization [32,33] of the exchange-correlation functional, which includes gradient correction (GGA), was employed. The pseudopotentials are constructed from the CASTEP database. The screening effect of core electrons is approximated by local density approximation (LDA), while the screening effect of valence electrons is taken care off by GGA. Reciprocal space integration over the Brilloin zone is approximated through a careful sampling at a finite number of *k*-points using the Monkhorst–Pack scheme [34]. In all calculations, the kinetic energy cutoff E_{cut} and the density of the Monkhorst–Pack *k*-point mesh were chosen high enough in order to ensure convergence of the computed structures and energetic. To obtain equilibrium structures for a given set of lattice constants, ionic and electronic relaxations were performed using the adiabatic or 'Born–Oppenheimer' approximation, where the electronic system is always in equilibrium with the ionic system. Relaxations were continued until the total energy had converged. Sampling of reciprocal space has been performed using $2 \times 2 \times 2$ *k*-point in the Brillouin zone with kinetic energy cutoff of 350 eV was used.

In the present study, all calculations with molecular boundary conditions have been carried out with DFT [35–38] using DMOL3 code of Accelrys. A gradient corrected functional BLYP [39,40] and DNP basis set [40] was used through out the calculation. Basis set superposition error (BSSE) was also calculated for the current basis set in nonlocal density approximation (NLDA). The theory for reactivity index calculations is mentioned elsewhere in details [20]. Single point calculations of the cation and anion of each molecule at the optimized geometry of the neutral molecule were also carried out to evaluate Fukui functions and global and local softness. The condensed Fukui function and atomic softness were evaluated using Eqs. (5) and (8), respectively. The gross atomic charges were evaluated by using the technique of electrostatic potential (ESP) driven charges.

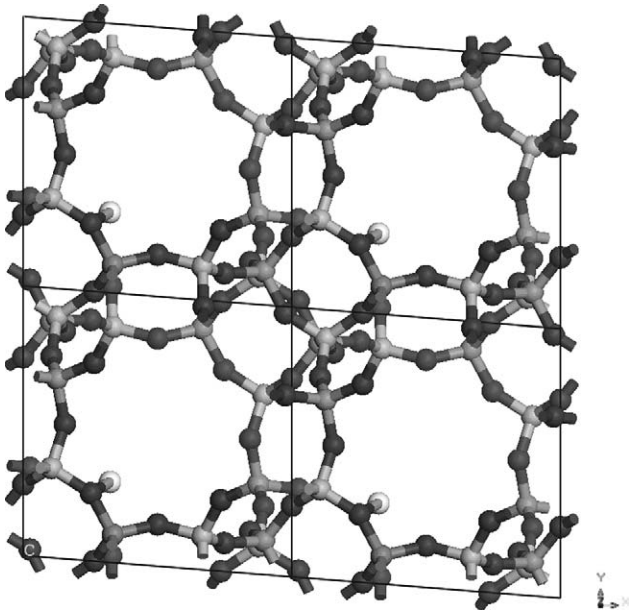

Fig. 1. The super cell model to represent bivalent metal AlPO-34 framework used for periodic calculation. This is an alternate network of Al and P connected through oxygen. One of the Al is replaced by a bivalent dopant. All the major atoms are labeled. For trivalent dopant the structure will be without this proton.

Calculations were performed on AlPO-34 framework, which is isostructural with zeolite chabazite. We have used 36 atoms to define the doped framework of MeAlPO-34 using the super cell approach. We have used one dopant per unit cell throughout this calculation. We have first relaxed the localized environment of the dopant only, to model the influence of the localized environment of the dopant. This is followed by the full structure relaxation excluding the first relaxed part; to model the effect of the dopant on its distant neighbors. The model of the super cell is shown in Fig. 1.

The cluster calculations were formed on localized cluster generated from the AlPO-34 structure as shown in Fig. 2 with the terminal Al or P. Two independent clusters of the formula (1) $M^{+2}AlP_2O_{12}H_9$ and (2) $M^{+3}AlP_2O_{12}H_8$ to represent the bivalent and trivalent dopant incorporated clusters, respectively, were developed. The proton is included at the bridging oxygen where the dopant is incorporated for electrical neutrality for bivalent substitution. The terminal Al or P were replaced by hydrogen at that distance to mimic the real situation. The models are shown in Fig. 3(a) and (b), respectively.

4. Results and discussion

We have first performed a periodic calculation with the metal dopants and AlPO framework to monitor the effect of the dopants in the framework structure in terms of geometric parameters like bond distances and angles. Substitution energy

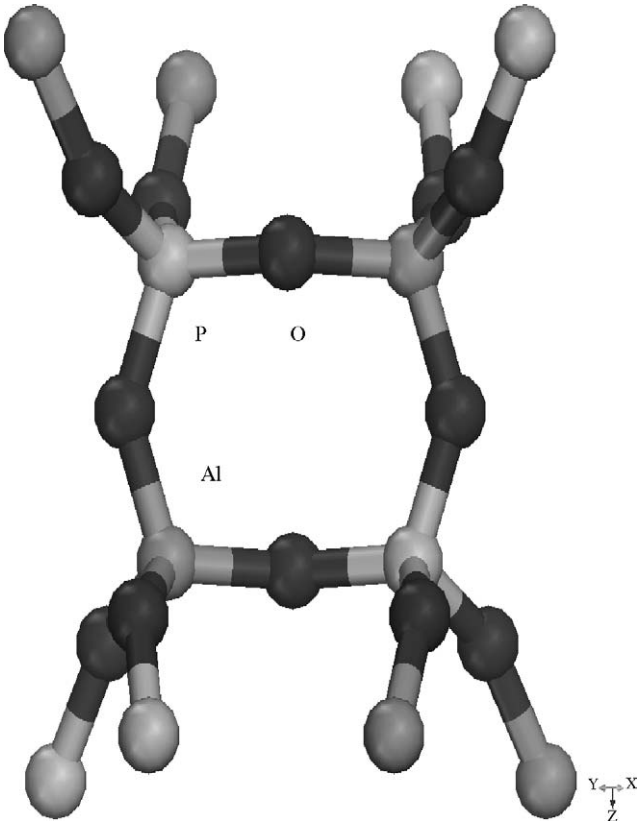

Fig. 2. The cluster model generated to represent AlPO-34 framework. This is as well a network of alternative Al and P connected through O. Each of the Al is connected to four other P and vice versa.

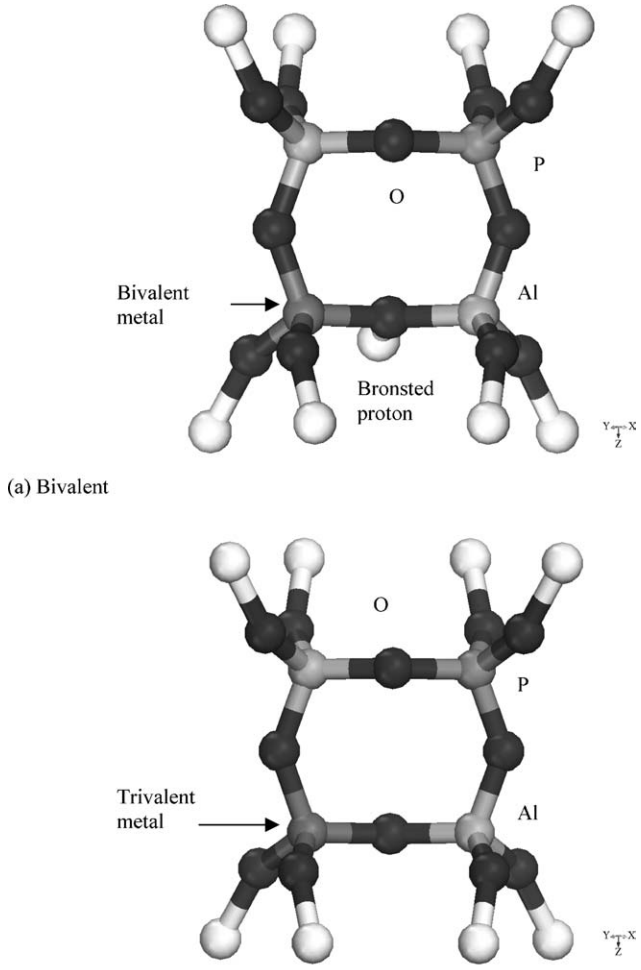

Fig. 3. Two independent cluster with the formula (a) $M^{+2}AlP_2O_{12}H_9$ and (b) $M^{+3}AlP_2O_{12}H_8$ to represent the bivalent and trivalent dopant incorporated clusters. The first cluster represents the bivalent dopant and the second one a trivalent dopant. The cluster termination here is with hydrogen.

for the dopants was also calculated. This is followed by reactivity index calculations based on localized structures to locate the active acid site for the MeAlPOs in terms of Brönsted and Lewis acidity. A semi-quantitative scale is proposed.

4.1. Local geometry of the dopants as observed form periodic calculation

As mentioned earlier we have used one dopant per unit cell, the metal dopants are kept at a distance of the unit cell dimension of the host framework (Fig. 1). This is to keep the spin interaction between the dopants and the framework negligible. All of the calculations were performed in P1 symmetry. The localized structure around the dopant was optimized initially and then the rest of the structure is relaxed except the previously relaxed part. This is to justify the relaxation effect caused by the dopant to the entire framework and as well to balance between CPU time and accuracy.

The ionic radii of the dopant cations were compared as shown in Table 1. The data show that among all the cations Co^{3+} is the smallest where as Mg^{2+} and Mn^{2+} have the highest ionic radii with the ionic radii of the rest lie in the range of 0.58–0.73 Å. The ionic radii of the cations falls in the order $Mn^{2+} = Mg^{2+} > Cr^{2+} > Fe^{2+} > Co^{2+}$ for bivalent cations and $Cr^{3+} > Al^{3+}$, $Mn^{3+} > Fe^{3+} = Co^{3+}$ for trivalent cations. The structural parameters to describe the local environment for bivalent dopants were summarized in Tables 2 and 3, respectively, whereas those data for trivalent metal dopants were shown in Tables 4 and 5, respectively. The distance between metal dopant (bivalent) and its four nearest neighbor-

Table 1
Ionic radii [50] of the dopants incorporated in AlPO-34 framework with a reference to Al^{3+}

Metal ion	Ionic radii (Å)
Al^{3+}	0.58
Co^{2+}	0.65
Co^{3+}	0.55
Mn^{2+}	0.83
Mn^{3+}	0.58
Mg^{2+}	0.83
Fe^{2+}	0.61
Fe^{3+}	0.55
Cr^{2+}	0.73
Cr^{+3}	0.62

Table 2
The M–O bond distance for the bivalent dopant cations with respect to the Al^{3+} cation as present in the optimized supercell of AlPO-34

M	M–O1	M–O2	M–O3	M–OH	⟨R⟩	Ref. [12]	Exp.
Mg^{2+}	1.85	1.88	1.86	2.19	1.94	1.93	1.94 [42]
Mn^{2+}	2.01	2.02	2.03	2.25	2.08	2.08	2.02 [43]
Cr^{2+}	1.99	2.03	2.04	2.36	2.11	2.11	–
Co^{2+}	1.89	1.94	1.95	2.24	2.00	1.99	1.94 [44]
Fe^{2+}	1.97	1.98	1.99	2.19	2.01	2.01	–
Al^{3+}	1.72	1.72	1.73	1.73	1.73	1.73	1.73 [45]

Table 3
The bond angles associated with the bivalent dopant cations with respect to the Al^{3+} cation as present in the optimized supercell of AlPO-34

M	M–OH–P	M–O–P	Al–O–P
Mg^{2+}	132.41	137.17	148.36
Mn^{2+}	127.81	135.06	147.89
Cr^{2+}	127.50	133.92	147.72
Co^{2+}	129.34	136.06	148.51
Fe^{2+}	128.97	135.77	148.54
Al^{3+}	148.59	148.59	148.59

Table 4
The M–O bond distance for the trivalent dopant cations with respect to the Al^{3+} cation as present in the optimized supercell of AlPO-34

M	M–O1	M–O2	M–O3	M–O4	⟨R⟩	Ref. [12]	Exp.
Mn^{3+}	1.85	1.88	1.90	1.91	1.88	1.88	1.85 [46]
Cr^{3+}	1.87	1.87	1.90	1.91	1.89	1.89	–
Co^{3+}	1.84	1.83	1.84	1.86	1.84	1.84	1.89 [44]
Fe^{3+}	1.87	1.85	1.88	1.88	1.87	1.86	1.86 [47]
Al^{3+}	1.72	1.72	1.73	1.73	1.73	1.73	1.73 [45]

Table 5
The bond angles associated with the trivalent dopant cations with respect to the Al^{3+} cation as present in the optimized supercell of AlPO-34

M	M–O–P	Al–O–P
Mn^{3+}	139.74	149.87
Cr^{3+}	142.95	147.65
Co^{3+}	141.94	149.15
Fe^{3+}	143.44	147.95
Al^{3+}	148.59	148.59

ing oxygen were monitored. One of the oxygen is protonated and that oxygen is labeled as –OH, the rest of the oxygens are labeled as 1, 2 and 3. ⟨R⟩ is the average M–O distance. The numbers were compared with available experimental values [41–45] and those of Saadoune et al. [12]. It is observed that for the bivalent dopants the local environment is a distorted tetrahedral. For all the cases the M–OH distance is the longest. The M–O distances are considerably longer than the Al–O distance when the AlPO material is undoped, showing that the dopants introduce a considerable amount of distortion in the system. This trend matches with the earlier theoretical calculation results [12]. We have over estimated the bond distances for Co^{2+} and Mn^{2+}, rest of our values in some cases are even somewhat better than the previous values.

The optimized bond angle values for bivalent dopants, using periodic calculation are shown in Table 3. M–OH–P represents the angles between the metal, hydroxyl oxygen and phosphorous, M–O–P is the average angle the dopant metal is making with all its nearest oxygen neighbors and phosphorous, while the Al–O–P is the average angle between alumina, all its neighboring oxygen and phosphorous. The results in Table 3 show that the M–OH–P angle distorts most. This is may be due to the fact that with increase in the dopant size the protonated oxygen is further relaxed due to the repulsion resulted from the dopant and reduces the M–OH–P angle. The T–O–P and Al–O–P angle values show that the observed structural distortion is not local and can be propagated beyond the nearest neighbor to the undoped region, which is in sharp contrast to the earlier results of Saadoune et al. [12].

The structural parameter data for trivalent metal dopants in terms of bond length and bond angle were shown in Tables 4 and 5, respectively. The experimental values were as well compared [41–45]. As in the trivalent dopant case there is no charge compensation required and hence there is no additional proton with the bridging oxygen. In Table 4 we have compared the individual M–O bond distances for four nearest oxygen neighbors of the dopants, the average M–O distance, the available experimental values and the results of Saadoune et al. [12]. The results show that they are in pretty good agreement with the earlier theoretical work [12]. The calculated values are overestimated compared to those of experiments. All the bond distances were much longer than the reference Al–O bond distance showing that the incorporation of dopants induces a distortion in the framework. The M–O–P represents the average of all the four angles the metal made with its nearest oxygen neighbors, whereas Al–O–P represents the angles with non-nearest neighbor oxygens. The values are shown in Table 5. The results suggest that M–O–P angle is most distorted for Mn^{3+} and all the values are lower than that of pure AlPO-34. Now, for the Al–O–P angle it is observed that all the angles for doped framework are deviated from the undoped framework by less than 1 °. This suggests that in case of trivalent metal cations the distortion of the structure is local and short-range. The deformation does not propagate to the neighboring atoms of the undoped region, which is markedly opposite to the findings of the bivalent metal dopant.

It is therefore proposed from the results of periodic calculation that structural deformation is associated with the nature of dopants in terms of local geometry. The nature of distortion (short-range or long-range) is heavily dependent on the charge of the dopant.

4.2. Substitution energy calculated for the substituted dopant using periodic calculation

The substitution energy for both bivalent and trivalent dopants, is calculated by the following expression. We have

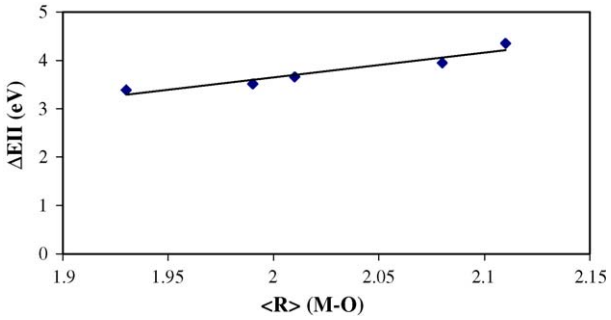

Fig. 4. Calculated substitution energy ΔE_{II} for the bivalent dopants as a function of $\langle R \rangle$ the average M–O distance.

Table 6
The global softness (in a.u.) for all the dopants present in the localized cluster model

Metal ion	Global softness (a.u.)
Co^{2+}	2.543
Co^{3+}	2.113
Mn^{2+}	2.674
Mn^{3+}	2.137
Mg^{2+}	2.324
Fe^{2+}	2.671
Fe^{3+}	2.351
Cr^{2+}	2.342
Cr^{3+}	1.989

used the unhydrated form of the metal cation as we are looking at the location of the dopants after calcinations only.

- For bivalent metal dopant the equation is

$$\text{AlPO-34} + \text{M(II)} \rightarrow \text{M}_{\text{II}}\text{HAlPO-34} + \text{Al}^{3+}$$

Then $\Delta E_{II} = [(E_{MIIHAlPO\text{-}34}) + (E_{Al^{3+}})] - [(E_{AlPO\text{-}34}) + (E_{MII})]$.

- For trivalent metal dopant the expression is

$$\text{AlPO-34} + \text{M(III)} \rightarrow \text{M}_{\text{III}}\text{AlPO-34} + \text{Al}^{3+}$$

Then $\Delta E_{III} = [(E_{MIIIAlPO\text{-}34}) + (E_{Al^{3+}})] - [(E_{AlPO\text{-}34}) + (E_{MIII})]$.

The energy for the isolated metal cation and the dopants were calculated by imposing the similar boundary condition as of the bulk. The substitution energy for the bivalent and trivalent cation is plotted against the average M–O distance as shown in Figs. 4 and 5, respectively. For the bivalent cation, the replacement energy increases with increase in the M–O distance. This shows that larger the distortion larger is the substitution energy. In case of the trivalent dopants the trend is same but for Cr^{3+} substitution energy remains very high compared to the rest of the dopant and hence may not be explained with the current analysis. This trend matches with the observation of Saadoune et al. [12] and we therefore assume that Cr^{3+} will rather prefer octahedral co-ordination than the tetrahedral co-ordination. There is a similar study with Cr by Rashkeev et al. as well [46] which has performed a study with Cr over alumina surface and figured out that for both varieties of alumina surface it is energetically favorable for Cr to occupy a subsurface layer position where it becomes six-fold coordinated. The relative large values of the substitution energy supports the phenomenon observed experimentally that AlPOs are unstable upon high metal doping. The substitution energy at this point allows predictions about the feasibility of dopant substitution, but it does not correlate with trends in the activity and therefore it is not possible to make prediction based on activity based on the computed substitution energy. This is the reason Saadoune et al. [12] therefore left the study as this point with a comment that the acidity of AlPOs is therefore not scalable. We therefore need to look at the local geometry and the electronic properties much carefully to propose the activity of the dopants in terms of Brönsted or Lewis acidity to rationalize this phenomenon. We will use the reactivity index calculation to monitor the same.

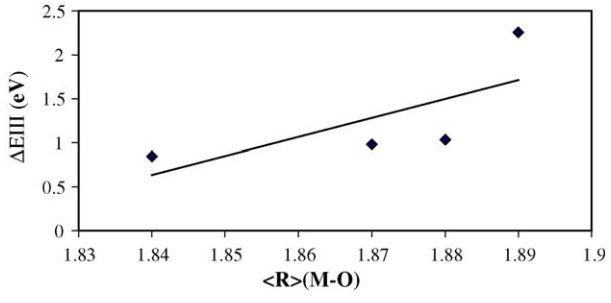

Fig. 5. Calculated substitution energy ΔE_{III} for the trivalent dopants as a function of $\langle R \rangle$ the average M–O distance.

4.3. Reactivity index calculation on localized clusters to predict acidity trend for these dopants

To explain the activity of the dopants in the AlPO-34 framework we have initially calculated the global softness for the dopants present in their respective clusters as shown in Table 6. There is no trend observed in the numbers generated. This expected behavior dictates that the global properties will be unable to correlate the activity of dopants, hence we performed localized reactivity index calculation for the bivalent dopants using $M^{+2}AlP_2O_{12}H_9$ cluster. This cluster involves a proton located at the bridging oxygen connecting the P and the dopant bivalent cation. The bivalent cation is substituted in place of Al^{3+}. The Fukui function and local softness for the hydroxyl proton is presented both in terms of nucleophilic and electrophilic activity. Roy et al. [47] have introduced relative electrophilicity (s_x^+/s_x^-) and relative nucleophilicity (s_x^-/s_x^+). These can be defined as the electrophilicity of any site as compared to its own nucleophilicity for the first term and vice versa. The site with highest (s_x^+/s_x^-) is the most probable site to be attacked by a nucleophile, and the site having the highest (s_x^-/s_x^+) ratio is the most probable site to be attacked by an electrophile. We have successfully used this parameter for both intermolecular and intramolecular interaction [48,49]. The results for Fukui function, local softness both in terms of nucleophilicity and electrophilicity as well the relative nucleophilicity trend is

Table 7
Fukui function, local softness and relative nucleophilicity for the bivalent dopants in terms of the hydroxyl proton using ESP charges calculated by DFT to monitor Brönsted acidity trend

Metal ion	f_x^+	s_x^+	f_x^-	s_x^-	s_x^+/s_x^-
Mg^{2+}	0.09	0.20	0.23	0.53	2.555
Mn^{2+}	0.14	0.37	0.12	0.32	1.156
Cr^{2+}	0.18	0.43	0.19	0.44	0.977
Co^{2+}	0.21	0.53	0.14	0.36	1.478
Fe^{2+}	0.20	0.53	0.16	0.44	1.204

shown in Table 7. It is observed that for some cases even when the local softness values are same the relative nucleophilicity values show a definitive trend. This is the trend observed in terms of the nucleophilicity of the hydroxyl proton and therefore this represents Brönsted acidity, and hence the trivalent dopants were not compared. The relative nucleophilicity is highest for Mg^{2+} and is lowest for Cr^{2+}, which is opposite to the trend observed in terms of substitution energy.

Fukui functions were used to monitor the dopants activity in terms of Lewis acidity. The results for local softness and relative nucleophilicity are shown in Table 8. We have used $M^{+3}AlP_2O_{12}H_8$ to monitor the Lewis acid activity for the dopants. Among the bivalent cations the results show that the maximum nucleophilicity is for Fe^{2+} and the lowest is for Mg^{2+}. For bivalent cation this order is totally different form the order obtained in terms of substitution energy and that obtained from the Brönsted acidity trend. For the trivalent dopant the highest nucleophilicity lies with Fe^{3+} and the lowest is for Mn^{3+}; the results matches with the trend of substitution energy. This can be explained from our earlier observation of the local geometries of the framework, after the substitution of dopant. For the bivalent dopant the distortion due to dopant incorporation is not localized and propagates beyond the local environment, whereas in case of trivalent metal dopant, the distortion is short-range and more localized. With the reactivity index results we therefore can postulate that for Brönsted acidity the long range interaction is playing the major role resulted mainly for bivalent dopants through the hydroxyl proton associated, where as for Lewis acidity, which is mainly occurring for trivalent metal cations the localized activity, is detrimental and hence the acidity trend for dopants is different. Hence, this acidity trend in AlPOs is scalable.

Table 8
Fukui function, local softness and relative nucleophilicity for the bivalent and trivalent dopants in terms of the dopant using ESP charges calculated by DFT to monitor Lewis acidity trend

Metal ion	f_x^+	s_x^+	f_x^-	s_x^-	s_x^+/s_x^-
Mg^{2+}	0.23	0.67	0.24	0.70	1.043
Co^{2+}	0.76	1.93	0.59	1.50	1.290
Co^{3+}	0.52	1.09	0.61	1.29	1.174
Mn^{2+}	0.32	0.85	0.41	1.09	1.282
Mn^{3+}	0.49	0.97	0.54	1.07	1.103
Fe^{2+}	0.53	1.42	0.71	1.91	1.347
Fe^{3+}	0.59	1.39	0.75	1.76	1.271
Cr^{2+}	0.63	1.47	0.49	1.15	1.284
Cr^{3+}	0.42	0.89	0.47	1.00	1.119

4.4. The correlation obtained so far to propose the semi-quantitative scale from the reactivity index study

We have performed a systematic study to analyze the activity of dopants in terms of Brönsted and Lewis acidity. We have used a combination of periodic and cluster calculation to propose a semi-quantitative scale for the dopants used in this study. First we have observed form ionic radii that for the bivalent dopants the order is $Mg^{2+} = Mn^{2+} > Cr^{2+} > Co^{2+} > Fe^{2+}$ and that for trivalent dopant is $Cr^{3+} > Mn^{3+} > Co^{3+} > Fe^{3+}$. Then we have compared their local geometries as obtained from periodic calculation. The average M–O bond distances for bivalent dopant are in the order $Cr^{2+} > Mn^{2+} > Fe^{2+} > Co^{2+} > Mg^{2+}$, where as the order for trivalent metal dopant is $Cr^{3+} = Mn^{3+} > Fe^{3+} > Co^{3+}$. It is observed that the M–OH distance is the most distorted for bivalent dopant. For both the dopants the structure undergoes some deformation after dopant substitution, but form the bond angles and especially from the Al–O–P angle it is observed that for bivalent dopant the distortion propagates to the area even where there is no dopant whereas for trivalent metal dopant it is more localized. This is in contradiction with the earlier work [12]. We then performed the substitution energy calculation for all the dopants. We have considered the metal in the unhydrated form and not in the hydrated phase as the AlPO materials used for catalysis is only after calcinations. This is another limitation of the Saadoune et al. [12] as they considered the hydrated complex to mimic the hydrothermal synthesis procedure, but the acidity of MeAlPOs is achievable after calcinations only during experiment, hence one need to consider the unhydrated phenomenon. The order of substitution energy for both bivalent and trivalent dopant is same as the order obtained for average M–O distance. This is logical as with increase in the M–O distance the dopant inclusion is a favorable one. We have as well seen that the substitution energy for trivalent dopant is much less than that of bivalent dopant. At this stage we were unable to predict any trend in terms of acidity as the substitution energy cannot be a meter to determine that; we therefore wanted to look at the local geometry more carefully. We therefore performed localized reactivity index calculation to monitor the relative nucleophilicity of the hydroxyl proton for bivalent dopant and the dopant itself for trivalent situation. As we have mentioned earlier that relative nucleophilicity is a better descriptor for prescribing a trend we have used that for the current prediction as well, which can as well be seen in Table 8 that even in some cases the local softness values are same for nucleophilic activity. The trend observed for bivalent dopant is $Cr^{2+} < Mn^{2+} < Fe^{2+} < Co^{2+} < Mg^{2+}$, which is in the same order but the progression order is just reversed. As this is in terms of the hydroxyl hydrogen this represents the Brönsted acid activity for the dopants and matches the trend observed experimentally [44]. For the Lewis acidity trend for all the dopants, the trend for bivalent dopant is $Fe^{2+} > Co^{2+} > Cr^{2+} > Mn^{2+} > Mg^{2+}$, which is totally different from the trend

for Brönsted acidity. The trend for trivalent dopant is $Fe^{3+} > Co^{3+} > Cr^{3+} > Mn^{3+}$. These two trends again match very well with the ionic radii of the dopants. The Lewis acidity trend for the dopants as well is comparable with the experimental trend [43]. Hence we can say that the local geometry and electronics combine to propose a scale and the reactivity index is the best candidate to explain the intermolecular level interactions more accurately that other methodologies.

5. Conclusion

This is the first study to propose a semi-quantitative scale to correlate the Brönsted and Lewis acidity resulted for a range of bivalent and trivalent dopants in MeAlPO-34. We have performed a combination of periodic and cluster calculation to correlate the effect of environment on the activity of dopants. The periodic calculation results show that the activity of hydroxyl proton is much more dependent on the environment as the distortion in the tetrahedral geometry propagates beyond the doping region. This phenomenon is not observed in case of non-protonated structures resulted from trivalent dopants. These results show us the distortion propagation or in other words the deformation resulted in the structure due to inclusion of the dopant can affect its nearest or next to nearest neighbor atom, which will further influence the activity resulted from the substitution of the dopant and hence the acidity. To visualize this effect one need to look more closely at the localized interaction at the close environment of the dopant atom. This can only be done through the localized reactivity index calculation. The relative nucleophilicity order for the active moiety in the AlPO cluster represents the trend nicely. We therefore can as well account for the acidity of AlPOs comprehensively. The trend for Brönsted acidity is $Cr^{2+} < Mn^{2+} < Fe^{2+} < Co^{2+} < Mg^{2+}$, where as the trend for Lewis acidity mainly for trivalent metal dopant is $Fe^{3+} > Co^{3+} > Cr^{3+} > Mn^{3+}$. This optimistic result encourages us to monitor a mixed valence situation, which may ideally exist during calcinations for the cations with variable oxidation state.

References

[1] M. Hartmann, L. Keven, Transition-metal ions in aluminophosphate and silicoaluminophosphate molecular sieves: location, interaction with adsorbates and catalytic properties, Chem. Rev. 99 (1999) 635–664.

[2] J.M. Thomas, Design, synthesis and in situ characterization of new solid catalysts, Angew. Chem. Int. Ed. 38 (1999) 3588–3628.

[3] A. Corma, H. Garcia, Organic reactions catalyzed over solid acids, Catal. Today 38 (1997) 257–308.

[4] R.A. Sheldon, I.W.C.E. Arends, H.E.B. Lampers, Activities and stabilities of redox molecular sieve catalysis in liquid phase oxidations a review, Czeck. Chem. Commun. 63 (1998) 1724–1742.

[5] P.A. Barrett, G. Sankar, C.R.A. Catlow, J.M. Thomas, Interaction of acetonitrile with cobalt-containing aluminophosphates: an X-ray absorption investigation, J. Phys. Chem. B 101 (1997) 9555–9562.

[6] R.A. Sheldon, J.K. Kochi, Metal Catalyzed Oxidation of Organic Compounds, Academic Press, New York, 1981.

[7] H. Nur, H. Hamdan, The ionic size of metal atoms in correlation with acidity by the conversion of cyclohexanol over MeAPO-5, Mater. Res. Bull. 36 (2001) 315–322.

[8] M. Hartmann, L. Kevan, Substitution of transition metal ions into aluminophosphates and silicoaluminophosphates: characterization and relation to catalysis, Res. Chem. Int. 28 (2002) 625–695.

[9] D.B. Akolekar, Multimetal-substituted aluminophosphate molecular sieves, Appl. Catal. A: Gen. 171 (1998) 261–272.

[10] R.A. Sheldon, J.K. Kochi, Metal Catalyzed Oxidations of Organic Compounds, Academic Press, New York, 1981.

[11] I. Saadoune, F. Corà, C.R.A. Catlow, Computational study of the structural and electronic properties of dopant ions in microporous AlPOs. 1. Acid catalytic activity of divalent metal ions, J. Phys. Chem. B 107 (2003) 3003–3011.

[12] I. Saadoune, F. Corà, M. Alfredsson, C.R.A. Catlow, Computational study of the structural and electronic properties of dopant ions in microporous AlPOs. 2. Redox catalytic activity of trivalent transition metal ions, J. Phys. Chem. B 107 (2003) 3012–3018.

[13] I. Saadoune, C.R.A. Catlow, F. Corà, Site ordering of dopant ions in microporous aluminophosphates—size effects, Microp. Mesop. Mater. 59 (2003) 161–165.

[14] R.G. Parr, R.G. Pearson, Absolute hardness—companion parameter to absolute electronegativity, J. Am. Chem. Soc. 105 (1983) 7512–7516.

[15] R.G. Pearson, Recent advances in the concept of hard and soft acids and bases, J. Chem. Edu. 64 (1987) 561–567.

[16] R.G. Parr, W.T. Yang, Density functional-approach to the frontier-electron theory of chemical-reactivity, J. Am. Chem. Soc. 106 (1984) 4049–4050.

[17] P. Geerlings, F. De Proft, HSAB principle: applications of its global and local forms in organic chemistry, Int. J. Quant. Chem. 80 (2000) 227–235.

[18] L.T. Nguyen, T.N. Le, F. De Proft, A.K. Chandra, W. Langenaeker, M.T. Nguyen, P. Geerlings, Mechanism of [2 + 1] cycloadditions of hydrogen isocyanide to alkynes: molecular orbital and density functional theory study, J. Am. Chem. Soc. 121 (1999) 5992–6001.

[19] A. Chatterjee, T. Iwasaki, T. Ebina, Reactivity index scale for interaction of heteroatomic molecules with zeolite framework, J. Phys. Chem. A 103 (1999) 2489–2494.

[20] A. Chatterjee, T. Ebina, T. Iwasaki, F. Mizukami, Intermolecular reactivity study to scale adsorption property of *para*- and *meta*-substituted nitrobenzene over 2:1 dioctahedral smectite, J. Chem. Phys. 18 (2003) 10212–10220.

[21] J.L. Gazquez, F. Mendez, The hard and soft acids and bases principle: an atoms in molecules viewpoint, J. Phys. Chem. 98 (1994) 4591–4593.

[22] A. Chatterjee, T. Iwasaki, T. Ebina, A. Miyamoto, Density functional study for estimating Brönsted acid site strength in isomorphously substituted ZSM-5, Microp. Mater. 21 (1998) 421–428.

[23] G. Sastre, A. Corma, Relation between structure and Lewis acidity of Ti-beta and TS-1 zeolites: a quantum-chemical study, Chem. Phys. Lett. 302. (1999) 447–453.

[24] R. Deka, R. Vetrivel, S. Pal, Application of hard–soft acid–base principle to study Brönsted acid sites in zeolite clusters: a quantum chemical study, J. Phys. Chem. A 103 (1999) 5978–5982.

[25] R. Deka, K. Hirao, Lewis acidity and basicity of cation-exchanged zeolites: QM/MM and density functional studies, J. Mol. Catal. A 181 (2002) 275–282.

[26] W. Yang, W.J. Mortier, The use of global and local molecular-parameters for the analysis of the gas-phase basicity of amines, J. Am. Chem. Soc. 108 (1986) 5708–5711.

[27] M.P. Teter, M.C. Payne, D.C. Allen, Solution of Schrödinger's equation for large systems, Phys. Rev. B 40 (1989) 12255–12263.

[28] M.C. Payne, M.P. Teter, D.C. Allen, T.A. Arias, J.D. Johannopoulos, Iterative minimization techniques for ab initio total-energy calculations—molecular dynamics and conjugate gradients, Rev. Mod. Phys. 64 (1992) 1045–1097.

[29] D. Vanderbilt, Soft self-consistent pseudopotentials in a generalized eigenvalue formalism, Phys. Rev. B 41 (1990) 7892–7895.

[30] J. Perdew, A. Zunger, Self-interaction correction to density-functional approximations for many-electron systems, Phys. Rev. B 23 (1981) 5048–5079.

[31] B. Winkler, V. Milman, M.C. Payne, Orientation, location, and total energy of hydration of channel H_2O in corderite investigated by ab initio total-energy calculation, Am. Mineral. 79 (1994) 200–204.

[32] J.P. Perdew, Density-functional approximation for the correlation energy of the inhomogeneous electron gas, Phys. Rev. B 33 (1986) 8822–8824.
[33] A.D. Becke, Density functional exchange energy approximation with correct asymptotic behavior, Phys. Rev. A 38 (1988) 3098–3100.
[34] H.J. Monkhorst, J.D. Pack, Special points for Brillouin-zone integrations, Phys. Rev. B 13 (1976) 5188–5192.
[35] B. Delley, An all-electron numerical-method for solving the local density functional for polyatomic-molecules, J. Chem. Phys. 92 (1990) 508–517.
[36] B. Delley, Analytic energy derivatives in the numerical local-density-functional approach, J. Chem. Phys. 94 (1991) 7245–7250.
[37] B. Delley, From molecules to solids with the DMol(3) approach, J. Chem. Phys. 113 (2000) 7756–7764.
[38] B. Delley, Modern density functional theory: a tool for chemistry, in: J.M. Seminario, P. Politzer (Eds.), Theoretical and Computational Chemistry, vol. 2, Elsevier Science, Amsterdam, 1995.
[39] A.D. Becke, A multicenter numerical-integration scheme for polyatomic-molecules, J. Chem. Phys. 88 (1988) 2547–2553.
[40] C.T. Lee, W.T. Yang, R.G. Parr, Development of the Colle–Salvetti correlation-energy formula into a functional of the electron-density, Phys. Rev. B 37 (1988) 785–789.
[41] G. Sankar, J.M. Thomas, C.R.A. Catlow, Combining, X-ray absorption with X-ray diffraction for the structural elucidation of catalysts, Top. Catal. 10 (2000) 255–264.
[42] P.A. Barrett, G. Sankar, C.R.A. Catlow, J.M. Thomas, High-pressure NMR relaxation study of the solute and solvent dynamics of undercooled aqueous tetraethylammonium bromide solutions, J. Phys. Chem. 100 (1996) 897–904.
[43] A. Tuel, S. Caldarelli, A. Meden, L.B. McCusker, C. Baerlocher, A. Ristic, N. Rajic, G. Mali, V. Kaucic, NMR characterization and Rietveld refinement of the structure of rehydrated $AlPO_4$-34, J. Phys. Chem. B 104 (2000) 5697–5705.
[44] F. Corà, G. Sankar, C.R.A. Catlow, J.M. Thomas, Electronic state and three-dimensional structure of Mn(III) active sites in manganese-containing aluminophosphate molecular sieve catalysts for the oxyfunctionalisation of alkanes, Chem. Commun. (2002) 734–735.
[45] C. Zenonos, G. Sankar, F. Corà, D.W. Lewis, Q.A. Pankhurst, F. Corà, C.R.A. Catlow, J.M. Thomas, On the nature of iron species in iron substituted aluminophosphates, Phys. Chem. Chem. Phys. 4 (2002) 5421–5427.
[46] S.N. Rashkeev, K. Sohlberg, M.V. Glazoff, J. Novak, S.J. Pennycook, S.T. Pantelides, Transition metal atoms on different alumina phases: the role of subsurface sites on catalytic activity, Phys. Rev. B 67 (2003) 115414.
[47] R.K. Roy, S. Krishnamurti, P. Geerlings, S. Pal, Local softness and hardness based reactivity descriptors for predicting intra- and intermolecular reactivity sequences: carbonyl compounds, J. Phys. Chem. A 102 (1998) 3746–3755.
[48] A. Chatterjee, T.M. Suzuki, Y. Takahashi, D.A.P. Tanaka, A density functional study to choose the best fluorophore for PET sensor, Chem. A: Eur. J. 9 (2003) 3920–3929.
[49] A. Chatterjee, T. Ebina, Y. Onodera, F. Mizukami, Effect of exchangeable cation on the swelling property of 2:1 dioctahedral smectite—a periodic first principle study, J. Chem. Phys. 120 (2004) 3414–3424.
[50] D.R. Lide (Ed.), CRC Handbook of Chemistry, CRC Press, New York, USA, 1975.